THE UNIVERSITY OF BRITISH COLUMBIA

Chemistry
Faculty of Science

COMPREHENSIVE EXAM REPORT

Exploration of Crystal Nucleation Phenomena Through Molecular Simulation

Author
Hayden SCHEIBER

Supervisor
Dr. Gren PATEY

Chair
Dr. Geoffrey HERRING

Committee
Dr. Yan WANG
Dr. Mark THACHUK
Dr. Keng CHOU

Date	**Time**	**Location**
April 29th, 2019	9:00 AM	CHEM D317

1 Introduction

There exists a vast set of chemically interesting questions that are extremely difficult to explore experimentally with currently available methods. Often the experiments needed to answer such questions can take years to design and properly execute. The difficulty in many such experiments arises due to the tiny length scales and/or very rapid time scales of the phenomena under consideration. On the other hand, computer simulation of chemical systems is a field that has flourished in recent years due to a combination of compounding factors. The rigorous theoretical framework continuously developed over the last hundred years or more, combined with the recent rapid development and advancement in computational power, has allowed computer simulation of dynamical chemical systems — known as molecular dynamics (MD) — to reach a new level of scientific possibility. We are now at a point where the current generation of theoretical chemists can confidently investigate chemically complex systems with unprecedented accuracy, often in relatively unexplored domains where physical experiments are most difficult to perform.

1.1 Nucleation Theory

The current report is concerned with a particularly formidable research topic: the nucleation mechanism of salts in water. Only in the last decade or so has computational power — and theoretical modeling — reached a point where this topic can realistically be explored through MD. Nucleation is defined as the first step in the spontaneous formation of new thermodynamic phases; it is a particularly troublesome process to explore experimentally due to the typical tiny size of nuclei combined with the complexity of the process. Proper experimental measurement of nucleation is challenging because crystal growth rates typically vary substantially as the size of the nucleus increases, and only larger crystals can be easily observed. Nucleation phenomena are conventionally described by classical nucleation theory (CNT).[1] CNT posits that the formation of nuclei is governed by two interactions: surface tension at the border of the nucleus, and internal interactions which are assumed equivalent to the bulk crystal. CNT therefore predicts that the free energy of a spherical nucleus (under constant pressure and temperature conditions) is given by

$$\Delta G(r) = \frac{4\pi r^3}{3}\rho\Delta g + 4\pi r^2\sigma, \tag{1}$$

where r is the radius of a nucleating cluster, $\frac{4}{3}\pi r^3$ is its volume, ρ is the number density of the potential nucleus, Δg is the Gibbs free energy difference between the crystal and solution phase per molecule, $4\pi r^2$ is the surface area of the nucleus, and σ is the surface tension of the interface. CNT does not necessarily require a spherical nucleus, but one is generally used in practice for mathematical convenience. CNT is often inadequate to fully describe the details of nucleation.[1] For instance, CNT predicts that nucleus formation is a one-step process but, in the case of lithium halides, preliminary MD studies show this not to be the case.[2,3] A complete mechanistic description of nucleation would have profound implications on a wide range of fields. Such fields include: chemical engineering, where nucleation is often undesirable; biochemistry, where protein crystallization is extremely important for X-ray characterization; and climate science, where water nucleation plays a critical role. In my research, I will explore this fundamental topic through MD investigation of lithium halides, as these are possibly among the simplest systems that nucleate through a non-classical (inconsistent with CNT) pathway.[3]

1.2 Molecular Dynamics

Although ab initio methods are very useful for generating accurate chemical and physical properties, they come at a very high computational cost for all but the smallest of systems. For example, without considering the exchange-correlation (XC) functional, density functional theory (DFT) scales in computational complexity with $\mathcal{O}(N^3)$, where N is the number of electrons. Other ab initio methods are even worse, making quantum-mechanical calculations of large chemical systems prohibitively complex. The theoretical study of nucleation phenomena requires that the simulation box size be large enough to eliminate (or greatly reduce) finite size effects which would otherwise contaminate the results. In practice, this requires thousands of atoms. Therefore, it is not currently viable to perform a fully quantum mechanical analysis of nucleation phenomena. Thankfully, atomic nuclei at temperatures around 300 K are both heavy enough and move fast enough such that many of their chemical properties can be accurately accounted for through Newton's classical equations of motion. Therefore, much less computationally costly *classical* MD simulations can be performed for the study of nucleation.

MD is a computational approach for simulating chemical systems based on Newtonian me-

chanics. In MD, time is discretized into quantities small enough as to realistically capture the details of atomic motions, generally in the range of $1 - 10\,\text{fs}$. Initial positions and velocities must be user defined, although initial velocities are often sampled randomly from a Boltzmann distribution of a chosen temperature. At each time step thereafter, the total potential energy of each interaction site is calculated as a summation of pre-defined interactions (or *models*) with every other site in the simulation, up to a given cutoff radius. In most cases this potential energy is calculated via *effective pair potentials*, where three-body or higher order interactions are not explicitly included. The total potential energy of the system U is therefore

$$U = \sum_i \sum_{j>i} u_{ij} + \sum_i \sum_{j>i} \sum_{k>j} u_{ijk} + \ldots \approx \sum_i \sum_{j>i} u_{ij}^{eff}. \tag{2}$$

Here, u_{ij} is the true two body interaction between site i and j. Each further term in this series is a sum of higher order many-body interactions. u_{ij}^{eff} is the effective two body interaction, which attempts to take into account the average affects of the three-body and higher interactions for a specific chemical environment. This approximation reduces the transferability of models, but facilitates a huge reduction in computational cost. The effective pair potentials are carefully chosen to govern the interactions between individual sites such that specific chemical properties of interest are expressed accurately. It is generally not possible to create a pairwise classical model that will accurately predict *all* chemical and physical properties for a particular species of interest.

Once the potential energy of each site is known, forces on each site $\vec{F}_i$ are calculated from the gradient ($\vec{\nabla}_i$) of the potential

$$\vec{F}_i(t) = -\vec{\nabla}_i u_i(\vec{r}_i, t) \tag{3}$$

where $u_i(\vec{r}_i, t)$ is the potential energy of site i at position $\vec{r}_i$ and time step t, calculated as a sum over individual interactions. From the forces and masses (m_i), accelerations ($\vec{a}_i$) are computed by Newton's second law,

$$\vec{a}_i(t) = \frac{\vec{F}_i(t)}{m_i} \tag{4}$$

which is numerically integrated through time to generate a trajectory. Additional constraints are often added between sites in bonded molecules to prevent the breaking of bonds.

1.3 Models

Before it is possible to properly explore any lithium halide nucleation phenomena through computational methods, a proper set of models for lithium halides in water — that *at the very least* capture the correct general physics of the situation — must be available. Presently, the existing empirical models for lithium halides are seriously flawed for the purposes of nucleation research. The two available models are the Jeung-Chetham[4] (JC) and Tosi-Fumi[5] (TF) models. In the JC model, potential energy is defined pairwise. Each pair interaction takes the form of

$$u_{ij}(r_{ij}) = \frac{1}{4\pi\varepsilon_0}\frac{q_i q_j}{r_{ij}} + 4\epsilon_{ij}\left[\left(\frac{\sigma_{ij}}{r_{ij}}\right)^{12} - \left(\frac{\sigma_{ij}}{r_{ij}}\right)^{6}\right]. \tag{5}$$

The first term is the standard Coulombic interaction between sites i and j with charges of q_i and q_j at separation distance r_{ij}; ε_0 is the vacuum permittivity. The second term is a Lennard-Jones (LJ) potential with well-depth parameter ϵ_{ij} and distance parameter σ_{ij}. The first term of the LJ potential represents (through a rather arbitrary functional form) Pauli repulsion between electron clouds, while the second term represents London dispersion. The particular parameters (ϵ_{ij} and σ_{ij}) between ions also depend on the choice of water model; for our study, we primarily focused on the parameters associated with the extended simple point charge (SPC/E) water model.[6] The JC models affiliated with other water models were examined, but performed even worse than those reported here. The TF model, while also a pairwise potential, takes on the somewhat different functional form of

$$u_{ij}(r_{ij}) = \frac{1}{4\pi\varepsilon_0}\frac{q_i q_j}{r_{ij}} + B_{ij}e^{-\alpha_{ij}r_{ij}} - \frac{C_{ij}}{r_{ij}^6} - \frac{D_{ij}}{r_{ij}^8}. \tag{6}$$

The TF potential contains four parameters for each different pair interaction: B_{ij}, α_{ij}, C_{ij}, and D_{ij}. An exponential function — which has theoretical justification[7] — serves as the repulsive term. Two dispersion terms also exist, representing fluctuating dipole-dipole and dipole-quadrupole interactions.

When executed in MD simulations, the TF model incorrectly predicts that the hexagonal *wurtzite* structure is the most stable crystal form of *all* lithium halides. This is a serious problem because in reality, all lithium halides exist naturally in the cubic rocksalt crystal structure, while the wurtzite structure has been shown to be metastable in LiCl, LiBr, and LiI.[8–10] Similarly, the JC model pre-

dicts that wurtzite is more stable in the case of LiBr and LiI, although it does predict the correct crystal structures for LiF and LiCl.[11] The parameters of the JC model were fit to solvation free energies, radial distribution functions, ion-water interaction energies, rocksalt lattice energies, and rocksalt lattice parameters at 300 K.[4] The TF parameters were fit to correctly predict equations of state, their derivatives, lattice parameters, and lattice energies for the rocksalt crystal structure.[5,12] However, the creators of both models did not realize that lower energy crystal structures would exist for their lithium halide models. Without prediction of the proper crystal structure, these models cannot be utilized to accurately explore more complex nucleation phenomena. Furthermore, the JC model predicts solubilities in LiF that are much greater than experimental values, which is a problem for proper simulation of nucleation.[3] Therefore, the first step of my research is to modify the current empirical models of lithium halides for nucleation research. While in pursuit of this, I have also examined why the rocksalt crystal structure is found so ubiquitously for simple salts in nature, whereas the wurtzite structure often appears in model systems.

In order to compare the validity of lithium halide empirical models in the context of the crystalline state, a reliable reference system must be assigned. Ideally, this reference system would originate from experimental data. However, there currently exists only a small collection of experimental data points per salt for the properties of interest (lattice energies and constants). These data points exist for the salts only in their equilibrium positions at ambient pressure and temperature, in the rocksalt crystal structure. Additionally, different techniques for the prediction of lattice energies yield somewhat different results,[4,13–15] with differences as large as 30 kJ mol^{-1}.

The only fully experimental lattice energies, which are used for comparison in this report, are those calculated (indirectly) through the Born-Haber cycle.[14,16,17] The Born-Haber cycle utilizes Hess's law to calculate the lattice *enthalpy* (ΔH_L°) in a roundabout way. This method requires summing together the following directly measurable quantities: the enthalpy of ionization for the cation; the (negative) electron affinity for the anion; the dissociation enthalpy of any species whose standard state is molecular; sublimation/vaporization enthalpy for any species whose standard state is not gaseous; and the (negative of the) heat of formation for the salt in question. From lattice enthalpy, the typical method[14,16] used to calculate the lattice *energy* (E_L) of an arbitrary

non-molecular salt M_aX_b through the Born-Haber cycle is

$$E_L = \Delta H_L^\circ - \left[a\left(\frac{3}{2} - 2\right) + b\left(\frac{3}{2} - 2\right)\right] RT. \tag{7}$$

Here R is the gas constant and T is the temperature used for the calculation of ΔH_L° (298 K). The terms proportional to RT include: contributions from the thermal vibrational energy of the crystal lattice; the translational energy of the gas phase ions; and the pressure-volume term of the gas phase ions. This calculation does not correct for zero-point vibrational energy, which is experimentally difficult to measure. It also ignores the crystal PV term, of which the magnitude is far below the uncertainty in these calculations. The approximations used in calculating E_L from ΔH_L overestimate the vibrational energy in lightweight salts, as this energy is assumed equal to the high temperature classical limit $3(a + b)RT$. Based on reported values of $H^\circ(298\,\mathrm{K}) - H^\circ(0\,\mathrm{K}) \approx E_{Vib}(298\,\mathrm{K})$ for LiF and LiCl,[18] we improved the vibrational energy corrections to the lattice energies of these salts. No such data is reported for LiBr and LiI, nor is any experimental data available for zero-point vibrational energy corrections of any lithium halide salt. Hence fully-experimental lattice energies cannot be accurately calculated for any lithium halide salt, only best-guesses based on classical approximations are reported.[14]

How can empirical models be improved when the lattice energy — let alone the specific interactions between atoms — cannot be accurately measured? The approach used in my research is to harness the powerful mathematical machinery of quantum mechanics. There are a multitude of quantum mechanical methods available for calculating molecular properties. These range from comparatively simple Hartree-Fock (HF) calculations to computationally heavy approaches like the coupled-cluster singles and doubles method with perturbative inclusion of triples.[19] For the purposes of calculating properties of infinite periodic crystalline structures, there are in practice fewer options available. The specialized nature of condensed phase structures constrains the use of computationally costly post-HF methods. In addition to the added computational complexity of periodic post-HF calculations, there are no high quality correlation-consistent Gaussian basis sets available that have been optimized for solid state calculations of lithium halides. Density functional theory (DFT), although generally less exact than post-HF methods, is therefore presently the most suitable ab initio method for the study of condensed phase periodic systems. In light of this,

estimates of the vibrational energy (including zero-point energy) were obtained from DFT harmonic calculations of finite-temperature vibrational energies.[20,21] Hence we were able to generate vibrationally-corrected experimental lattice energies, which are reported later in Tables 3 to 6.

1.4 Overview of HF and DFT

Both HF theory and DFT are methods fundamentally concerned with solving the time-independent Schödinger equation for an arbitrary chemical system of N electrons and M nuclei,

$$\widehat{\mathcal{H}}\Psi(\vec{r}_1,\ldots,\vec{r}_N,\vec{R}_1,\ldots,\vec{R}_M) = E\Psi(\vec{r}_1,\ldots,\vec{r}_N,\vec{R}_1,\ldots,\vec{R}_M), \tag{8}$$

where Ψ is the total wavefunction of the system, $\vec{r}_i$ are the coordinates for electron i, $\vec{R}_A$ are the coordinates for nucleus A, E is the total energy, and $\widehat{\mathcal{H}}$ is the Hamiltonian operator of the system. Note that by starting from the Schödinger equation, we have already neglected relativistic effects. These effects tend to become non-negligible in the core electrons of heavy atoms, where the electrons approach moderate fractions of the speed of light. We have also neglected any internal nuclear structure, approximating the nuclei as single particles (not the collection of subatomic particles that they really are). This is a reasonable approximation because nuclei are extremely localized compared to electrons. In Hartree's atomic units — where Planck's constant is unity, the electron mass is unity, the elementary charge is unity, and the vacuum permittivity is $\frac{1}{4\pi}$ — the Hamiltonian of our system is

$$\widehat{\mathcal{H}} = -\frac{1}{2}\sum_{i=1}^{N}\nabla_i^2 - \frac{1}{2}\sum_{A=1}^{M}\frac{1}{M_A}\nabla_A^2 + \sum_{i=1}^{N}\sum_{j>i}^{N}\frac{1}{r_{ij}} + \sum_{A=1}^{M}\sum_{B>A}^{M}\frac{Z_A Z_B}{R_{AB}} - \sum_{i=1}^{N}\sum_{A=1}^{M}\frac{Z_A}{r_{iA}}. \tag{9}$$

Here, ∇_i^2 is the Laplacian operating in the spacial coordinates of electron i, M_A is the mass of nucleus A, Z_A is the atomic number of nucleus A, $r_{ij} = |\vec{r}_i - \vec{r}_j|$, $R_{AB} = |\vec{R}_A - \vec{R}_B|$, and $r_{iA} = |\vec{r}_i - \vec{R}_A|$. The five summations represent in order: the kinetic energy of the electrons; the kinetic energy of the nuclei; the electron-electron interaction energy; the nuclear-nuclear interaction energy, and the electron-nuclear interaction energy.

There are no methods for solving such a complicated eigenvalue problem as Eq. (8) in general. However, progress has been made via the Born-Oppenheimer (BO) approximation, in which the

motion of electrons and nuclei are treated as separable. This approximation is valid because the mass of electrons is considerably less than that of even the lightest nuclei. Hence, the electrons move much faster than the nuclei and can continuously re-equilibrate with nuclear movement. Mathematically, this idea is expressed as

$$\Psi(\vec{r}_1, \ldots, \vec{r}_N, \vec{R}_1 \ldots, \vec{R}_M) = \Psi_{elec}(\vec{r}_1, \ldots, \vec{r}_N; \vec{R}_1 \ldots, \vec{R}_M)\Psi_{nucl}(\vec{R}_1, \ldots, \vec{R}_M), \tag{10}$$

where the electronic wavefunction depends explicitly on the electronic coordinates, but only parametrically on the nuclear coordinates. Upon separation of the wavefunction, it becomes possible (after disregarding the cross kinetic energy terms[19]) to separate the Schrödinger equation into electronic and nuclear parts. The electronic part is

$$\widehat{\mathcal{H}}_{elec}\Psi_{elec} = E_{elec}\Psi_{elec}, \tag{11}$$

where

$$\widehat{\mathcal{H}}_{elec} = -\frac{1}{2}\sum_{i=1}^{N}\nabla_i^2 + \sum_{i=1}^{N}\sum_{j>i}^{N}\frac{1}{r_{ij}} - \sum_{i=1}^{N}\left(\sum_{A=1}^{M}\frac{Z_A}{r_{iA}}\right). \tag{12}$$

The terms corresponding to nuclear-nuclear repulsion and nuclear kinetic energy are separated out. In the electronic Hamiltonian, dependence on nuclear coordinates is made parametrically through the third Coulombic term.

Quantum chemistry methods are generally concerned only with the electronic component of the Schrödinger equation, where the nuclear component is often discarded in favour of a classical approximation. Indeed, both DFT and HF theory are approximations used to solve the electronic problem. An important consequence of this separation is that any eigenvalues of the electronic Hamiltonian do not include nuclear vibrational, rotational, or translational energy.

It is at this stage that the methods of HF theory and DFT diverge. In Hartree-Fock theory, the electronic wavefunction is made antisymmetric with respect to exchange of any two electrons (in agreement with the Pauli exclusion principle) by insisting that the total electronic wavefunction be a Slater determinant. This introduces an exchange term into the final HF equation, which exists only between electrons of the same spin. The HF equation can be interpreted as an equation for the allowed energies and wavefunctions of a single electron in the average electric potential

introduced by all $N-1$ other electrons and M frozen nuclei. In practice, the HF equation is a non-linear matrix eigenvalue problem expanded in a set of basis functions, where the elements of the Hamiltonian matrix depend on the occupied one-electron orbitals. Therefore, an initial guess for the electronic wavefunction is required to construct the so-called Fock matrix, which is diagonalized to produce a new set of electron orbitals (the eigenfunctions) and energies (the eigenvalues). These orbitals are input back into a new Fock matrix and the process is repeated until self-consistency is reached between cycles. Self-consistency is usually defined by a threshold difference in the total energy between cycles. See Ref. 19 for details.

Density functional theory, in on the other hand, is a reformulation of the electronic problem. The equations of DFT are written as *functionals* of the total electron density $\rho(\vec{r})$. In 1964, Hohenberg and Kohn[22] proved two theorems that demonstrated the legitimacy of DFT as a method for computing quantum mechanical properties. The first theorem shows that the external potential (i.e. the potential from the nuclei) acting on a fully-interacting system of N electrons is determined (up to an additive constant) by the electron density in its ground state. The second theorem is a proof of the variational principle in terms of electron density,

$$E_0\left[\rho_0\right] \leq E[\rho], \tag{13}$$

where $E_0\left[\rho_0\right]$ is the true electronic ground state energy as a functional of the ground state electron density ρ_0, and $E[\rho]$ is the energy resulting from ρ, an arbitrary electron density distribution. The equality is only satisfied if $\rho = \rho_0$.

The theorems of Hohenberg and Kohn paved the way for the formalization of DFT in 1965 with the Kohn-Sham (KS) method.[23] This groundbreaking paper introduced a fictitious non-interacting system of electrons with the same density as the interacting real system, leading to an eigenvalue equation. KS DFT is *in principle* an exact solution to the electronic problem, given an exact form of the XC functional. The XC functional is meant to encompass all of the many-particle correlation interactions that are absent in the rest of the equation. In the fifty years since the Kohn-Sham method was introduced, hundreds of XC functionals have been constructed, yet an exact form remains unknown. As was the case in the HF equation, the KS Hamiltonian depends on the occupied KS orbitals. Therefore, an iterative procedure is used until self-consistency is reached.

2 Methods

2.1 Ab Initio Calculations

Although fairly accurate experimental lattice energies are available, detailed experimental data for non-equilibrium lithium halide structures is unavailable. With that in mind, we turn to *ab initio* methods to probe the space of lithium halide structures. By exploring in detail the energy hyperspace of these salts, we are not only able to construct reliable reference states for MD model building, but we are also able to tease apart the delicate factors that determine crystal structure stability, while simultaneously exploring regions of phase space that are experimentally difficult to reach.

In principle, constructing an ab initio reference system to approximate the lattice energy is fairly simple. One first calculates the total energy per unit cell of the infinite crystalline system under the BO approximation E_{Total}, then separately the electronic energy of all ions in the unit cell are calculated in isolation

$$E_{Ions} = \frac{N}{2} E_{Anion} + \frac{N}{2} E_{Cation}, \tag{14}$$

where N is the number of atomic nuclei per unit cell while E_{Anion} and E_{Cation} are the total energies of the lone anion and cation, respectively. The two energies are then subtracted to yield

$$E_L = E_{Total} - E_{Ions}, \tag{15}$$

where E_L is the theoretical lattice energy per mole of ion pairs at 0 K. The term lattice energy may or may not include the zero point energy. In the context of this report, we shall define lattice energy as the underlying potential energy of the crystal lattice, with the zero point vibrational energy completed removed. The zero of energy is just the energy of the infinitely separated ions.

In practice, the construction of our quantum-mechanics based reference system was a slow and arduous process primarily because it required calculation of the energy in an infinitely periodic crystalline system, which necessitates special consideration in all aspects of the calculation. In our case, ab initio calculations were performed using the CRYSTAL17 software package,[24,25] an

HF/DFT-based quantum chemistry program specifically designed for infinite crystalline matter calculations. CRYSTAL17 uses atom-centered Gaussian basis sets, extended as Bloch functions.[25] For condensed matter quantum mechanical computations, the choice of basis set is usually the most important step.[25,26] Periodic Gaussian basis sets are one of two basis set choices used in solid state ab initio calculations, the other being plane waves. A discussion of the pros and cons of both basis set types can be found in Ref. 27. One problem commonly associated with Gaussian basis sets is their poor transferability from molecular to periodic systems. Due to the compacted nature of periodic systems, ab initio calculations generally require specially optimized Gaussian basis sets.[26]

For all crystalline ab initio calculations performed here — except those used to compare basis set effects — we adopted a recently created, triple-zeta valence quality solid-state basis set known as pob-TZVP,[26,28] the acronym means: Peintinger-Oliveira-Bredow (the authors) Triple-Zeta Valence with added Polarization functions. This basis set is available for all elements used in our study, and was optimized for the solid state through Kohn-Sham DFT calculations with a modified Perdew-Wang (PW) hybrid XC functional called PW1PW.[29]

For the calculation of lone ion energies, E_{Ions} in Eq. (14), the pob-TZVP basis set was not a good choice due to the lack of diffuse basis functions and optimization to a crystalline environment. For the energy calculation of reference lone ions, we used the triple-zeta valence quality molecular basis set upon which pob-TZVP is derived, called def2-TZVP,[26,30] which stands for "default version 2 - Triple Zeta Valence with added Polarizable functions." We also augmented the basis set with diffuse (D) functions in the outer orbitals, hence we will refer to the ion basis set as def2-TZVPD. As an indication of the importance of basis set in lattice energy calculation, Fig. 1 shows the difference between (fully optimized) rocksalt and wurtzite lattice energies for three basis sets. Only the pob-TZVP properly predicts the rocksalt crystal structure for all four lithium halides. In all cases, the def2-TZVPD basis set was used to calculate the energy of the lone ions. The "7-311G" basis set is a collection of medium quality crystalline basis sets: see Ref. 31 (Li), 32 (F), 33 (Cl), 34 (Br and I). The STO-3G (Slater Type Orbital - 3 Gaussians) basis sets are minimum quality molecular basis sets: see Ref. 35 (Li and F), 36 (Cl), 37 (Br), 38 (I). Two different exchange-correlation functionals were tested: PBE[39] and PW1PW.[29] Dispersion corrections are not included here.

It is often impossible to determine *a priori* which particular choice of XC functional will work

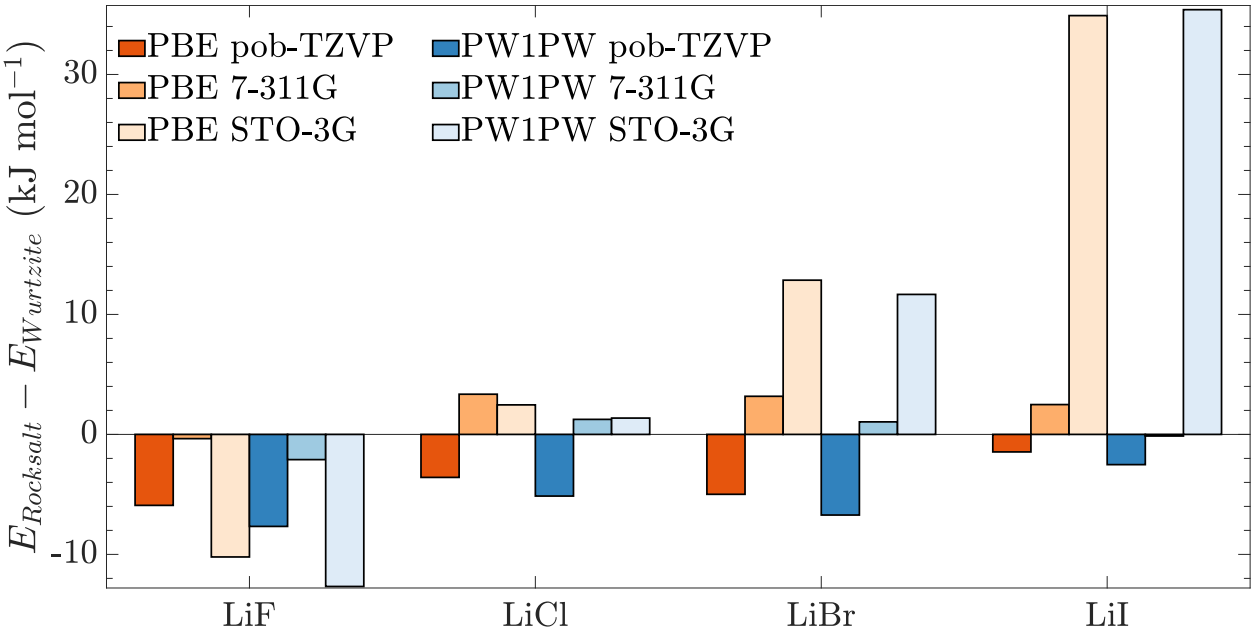

Figure 1: The dependence on the difference between rocksalt and wurtzite lattice energies on the basis set used. Experiment suggests all lithium halides should have negative values here, which is only reflected in the high quality pob-TZVP basis set.

best for a system of interest. With this in mind, we attempted ab initio calculations of solid state lithium halides using an array of different XC functionals from each rung of "Jacob's Ladder"[40] except double-hybrid (which incorporates post-HF calculations). In particular, we compared pure HF calculations and DFT calculations using XC functionals with the local density approximation (LDA), generalized gradient approximation (GGA), meta-GGA approximation, and global hybrid level of theory (which combines a component of pure HF exchange with DFT). Our choice of which XC functionals to test was in part based on whether or not empirical dispersion parameters for third generation dispersion[41,42] with Becke-Johnson damping[43,44] — hereafter referred to as D3(BJ) dispersion — were available. Refer to table 1 for a summary of XC functionals used.

In our case pure restricted HF calculations were included as an upper bound on the true lattice energy, since the crystal lattice is expected to have lower correlation energy than the ions. On the other hand, LDA XC functionals are known to overestimate bonding energy in most situations.[54,55] Therefore, we expect that the SVWN[45,46] (Dirac-Slater exchange with Vosko-Wilk-Nusair correlation) DFT calculations act as a lower bound on the calculated lattice energy.

We chose the PBE XC functional[39] as a representative for the GGA level of theory for several reasons. Most importantly, the PBE XC functional is a fully ab initio XC functional. It incorporates

Acronym	Theory Level	D3(BJ)	References
HF	HF	N	
SVWN	DFT LDA	N	45, 46
PBE	DFT GGA	Y	39
M06L	DFT Meta-GGA	N	47
M062X	DFT Global Hybrid	N	48
M06	DFT Global Hybrid	Y	48
B3LYP	DFT Global Hybrid	Y	49, 50, 51
HSE06	DFT Range-Separated Hybrid	Y	52
HSEsol	DFT Range-Separated Hybrid	Y	53
PW1PW	DFT Global Hybrid	Y	29

Table 1: List of exchange-correlation functionals compared in our study. Column three indicates whether or not dispersion parameters are defined for the D3(BJ) dispersion correction.[41,42]

electron density as well as its gradient at each point in space into the functional. The parameters set in the PBE functional are optimized with respect to other theoretical methods, rather than experiment. However, PBE usually overestimates bonding distances and lattice parameters in practice.[55]

For the Meta-GGA level of theory, we utilized the Minnesota 2006 series of XC functionals (M06,[48] M06L,[47] and M062X).[48] These exchange correlation functionals incorporate kinetic energy density into their complex functional forms. The M06 and M062X functionals also include HF exchange, making them global hybrid functionals.

At the global hybrid level of XC approximation, we tested an additional four XC functionals. The first of these is the extremely popular global hybrid functional known as B3LYP. The B3LYP functional was developed in the 1980's and utilizes Becke's three parameter exchange functional[49] which includes 20% HF exchange, 8% Slater LSDA exchange,[45] and 72% Becke-88 GGA exchange.[50] The correlation component of the functional is that of Lee, Yang, and Par (LYP)[51] containing 19% VWN1RPA[46] (Vosko-Wilk-Nusair random phase approximation) LDA correlation and 81% LYP GGA correlation. The LYP correlation functional was constructed from ab initio calculations of Helium.

In addition to the B3LYP functional, we also tested two Heyd-Scuseria-Ernzerhof (HSE) range-separated hybrid functionals: HSE06,[52] and HSEsol.[53] These XC functionals were developed specifically to improve computational efficiency in large systems by screening the non-local HF exchange with an error function and associated cutoff distance. The HSE XC functional is based

on the PBE XC functional,[39] while the HSEsol functional is based on the PBSsol XC functional.[56] Finally, we chose to test the PW1PW[29] hybrid functional because the pob-TZVP basis set was optimized using this XC functional. In the PW1PW hybrid XC functional, the exchange functional contains 20% HF exchange and 80% Perdew-Wang exchange.[57] PW1PW uses the Perdew-Wang correlation functional.[57]

As a test of the efficacy of the XC functionals for our purposes, we utilized CRYSTAL17's geometry optimization algorithm[25] to systematically optimize the geometry of rocksalt and wurtzite infinite lattices for each XC functional separately. For these and all subsequent ab initio condensed phase calculations, the pob-TZVP basis set was used. Fig. 2 shows a comparison of the difference in lattice energy between rocksalt and wurtzite geometry optimized crystal structures. It's clear that the XC functional is far less important to the outcome of DFT solid state calculations than the basis set is, although some calculations are clearly better suited than others for our purposes: both HF and B3LYP calculations predict incorrect structures for LiCl, LiBr, and LiI. One important point to note in these calculations is that the difference in energy between rocksalt and wurtzite is calculated to be on the order of $10\,\mathrm{kJ\,mol^{-1}}$, whereas the lattice energies themselves are on the order of $1000\,\mathrm{kJ\,mol^{-1}}$. It's not too surprising that it is difficult to achieve good accuracy when subtracting two very large numbers with a small difference.

Ab initio calculations require only a small set of input parameters. Since the HF or KS-DFT equations cannot be solved analytically, the equations must be solved numerically. Furthermore, they must be solved through an iterative self-consistent field (SCF) approach. Therefore, a set of tolerances must be defined that specify the numerical accuracy required and specify when the iterative approach has sufficiently converged. For the calculations in this research, we eventually settled on two reliable sets of input parameters to use, depending on the type of output data required. For normal single point energy calculations like those use to produce the potential energy surfaces, SCF equations were considered sufficiently converged once the change in total energy per unit cell between cycles was less than $10^{-8}\,\mathrm{E_H}$ (Hartree natural energy units). However, during geometry optimization and vibrational analysis calculations, the convergence requirements were set much tighter at $10^{-11}\,\mathrm{E_H}$ between SCF cycles.

Periodic ab initio calculations require that a grid of points be defined in reciprocal space for the purposes of calculating the wavefunctions and energies of an infinitely periodic lattice. In

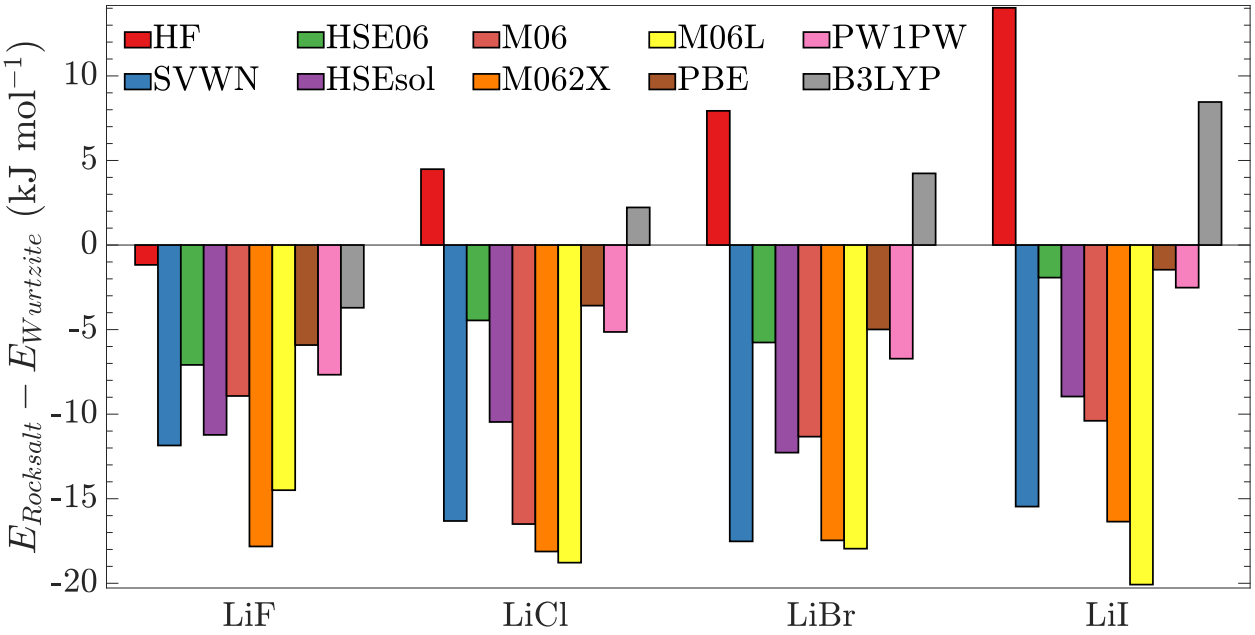

Figure 2: A comparison of the difference in lattice energy between rocksalt and wurtzite crystal structures vs the type of XC functional used. HF calculations are also shown for comparison. The pob-TZVP basis set was used here for all crystalline calculations. Dispersion corrections are not included here. Negative values favour rocksalt, in agreement with experiment.

CRYSTAL17, these sample points are used to approximate integrals over the irreducible part of the first Brillouin zone (BZ) when calculating crystal orbital energies. This grid is constructing using the Pack-Monkhorst method[58] in which a commensurate grid of k-points is selected, based on an input "shrinking factor". This shrinking factor F_S is used to generate a $F_S \times F_S \times F_S$ grid of k-points which span the reciprocal lattice unit cell. Only k-points which fall within the irreducible BZ are then selected as sample points for energy band calculations. The energy between these sample points is interpolated. Due to the symmetry properties of the first BZ, integration over the irreducible BZ results in a substantial reduction in the number of k-points that need to be sampled. For our calculations, we chose $F_S = 12$, which translates to 72 sample k-points for the rocksalt crystal structure, or 133 sample k-points for the wurtzite crystal structure.[25] In preliminary studies, this value was found to be the minimal shrinking factor that reliably produced accurate energies (compared with larger shrinking nets).

	LiF	LiCl	LiBr	LiI
Rocksalt	-1.65	-0.69	-0.64	-4.88
Wurtzite	-1.36	0.28	1.00	-1.04

Table 2: BSSE energy estimation (kJ/mol) of lithium halide salts in their equilibrium geometries for rocksalt and wurtzite crystal lattices. Calculated using the counterpoise method,[60] with the def2-TZVPD basis set[26,30] and PBE XC functional.[39]

2.1.1 Basis Set Superposition Error

Basis set superposition errors (BSSE) are a possible source of error that occurs due to incompleteness of a calculation's basis set. In the limit of a complete basis set, such errors are eliminated. Since practical ab initio calculations cannot use a complete basis set (it would need to be infinite), errors in lattice energy prediction arise when atom-centered basis functions overlap. This overlap of basis functions allows more variational freedom to describe all of the interacting atoms in their bonded state than was available to the individual non-interacting atoms. BSSE thus predict unrealistically strong bond/lattice energies in ab initio calculations done with small or non-optimized basis sets. There currently exists two primary methods available for estimation of BSSE in chemical systems: Mayer's chemical Hamiltonian approach[59] (unavailable in CRYSTAL17) or the Boys and Bernadi counterpoise (CP) method.[60] Different variations of the CP method exist,[61] but are not either not applicable to our calculations, or not available within the CRYSTAL17 code. Therefore, we used the CP method to estimate the BSSE for our lattice energies.

Since our atomic calculations were done using the def2-TZVPD basis set, we used this for our CP calculations. Table 2 lists the resulting estimated BSSE corrections for all lithium halides in both rocksalt and wurtzite configurations at their equilibrium geometries, using the PBE XC functional. Other exchange-correlation functionals were tested as well, with similarly small corrections. These results are a good indication that our chosen atomic basis set is near the basis set limit. We considered the size of these corrections small enough that all further calculations neglect these BSSE estimates.

2.1.2 DFT Dispersion Correction

The most difficult aspect of solving the Schrödinger equation within the BO approximation is correctly capturing the dynamical Coulombic interactions between electrons, known as the corre-

lation energy. It is from these electron correlations that the entirety of the dispersion interaction arises. The introduction of an exact correlation energy is the goal of all post-HF methods. Additional electron correlation between electrons of the same spin — due to exchange anti-symmetry — is simpler to account for mathematically and is known as exchange energy. The HF method introduces an exact exchange interaction via the exchange integrals but ignores correlation (by definition). Both the exchange and correlation energies are approximated in DFT through the XC functional, which is not exact. XC functionals tend not to properly capture the long-distance behaviour of the dispersion interaction.[42]

In an attempt to compensate for the lack of exact dispersion in DFT, several theoretical approaches have been introduced.[62] The most advanced of which is arguably D3(BJ) dispersion,[41–44] which adds an additional dispersion energy to the total energy calculated from DFT. The dispersion energy is calculated based on the particular XC functional used and the geometry of the system.[42] When D3(BJ) dispersion is introduced into the present lattice energy calculations, there is a lowering of the lattice energies for both rocksalt and wurtzite structures. However, the lowering of the lattice energies is more for rocksalt than for wurtzite, as can be seen in Fig. 3. Notice the change as compared with Fig. 2. To see if the D3(BJ) dispersion energy brought our calculations closer to experimental values, we compare the difference in experimental lattice energy[14] with our calculated rocksalt lattice energies in Fig. 4 and 5. In Fig. 4, the D3(BJ) dispersion energy is not included, while in Fig. 5 it is introduced. There is a clear improvement in the calculated lattice energies as a result of the added dispersion energy. We also examined the effect of D3(BJ) dispersion on lithium halide lattice parameters, as compared with very accurate experimental X-ray crystallography data. This data was measured at 298 K and is reported in column two of Table 1.3 in Ref 63. In this case there is less improvement; however, thermal expansion effects may decrease the gap and is a possibility we are currently investigating. One should note that the differences between theoretical and experimental lattice parameters are still very small compared with their absolute values, with errors on the order of 1%.

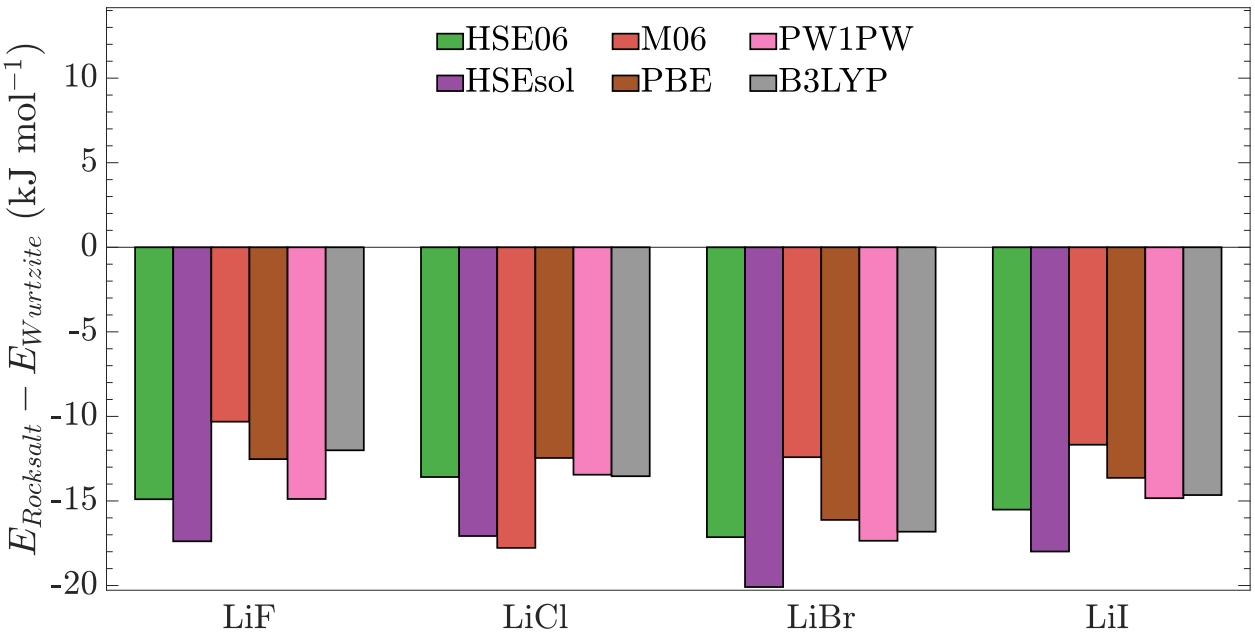

Figure 3: A comparison of the difference in lattice energy between rocksalt and wurtzite crystal structures vs the type of XC functional used, for XC functionals with defined D3(BJ) parameters. D3(BJ) dispersion energy was included for these calculations. Negative values favour rocksalt, in agreement with experiment.

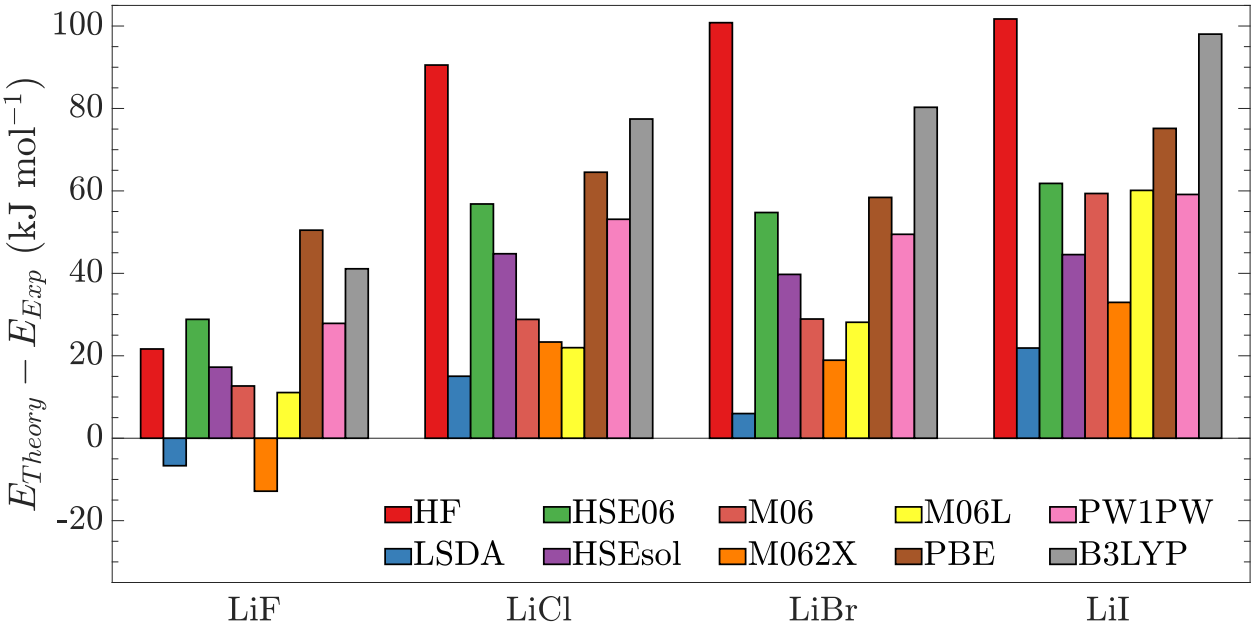

Figure 4: A comparison of the difference in lattice energy between theoretical and experimental lithium halides in the rocksalt crystal structure. D3(BJ) dispersion energy was not included in these calculations. Values closer to zero match experiment better.

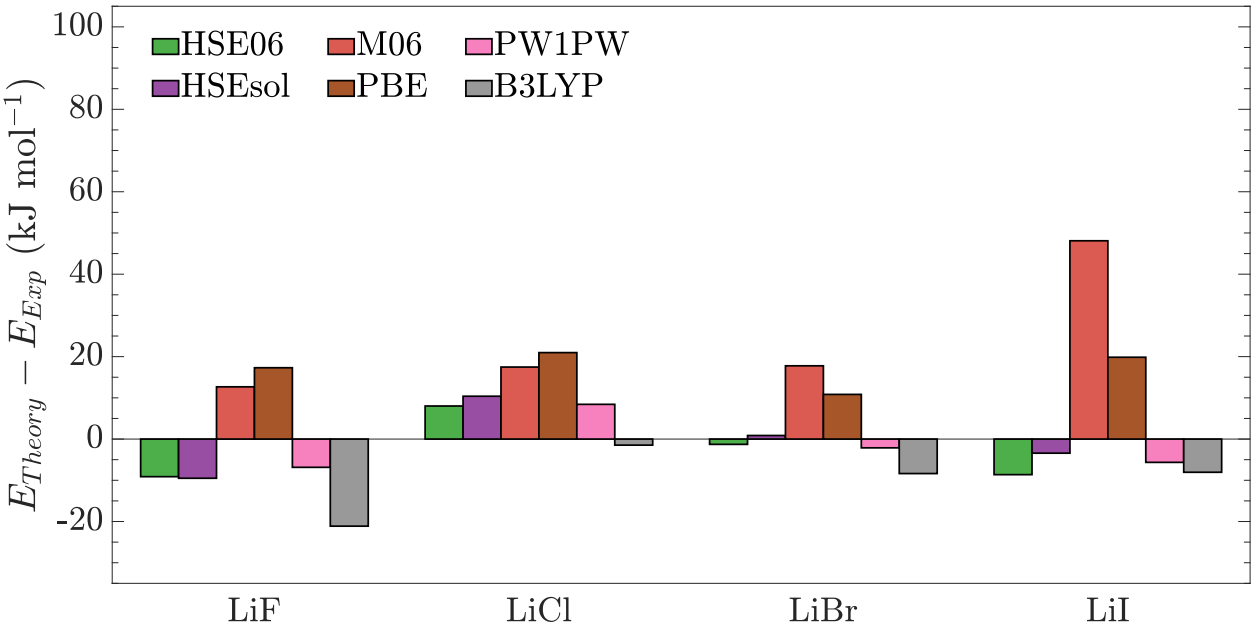

Figure 5: A comparison of the difference in lattice energy between theoretical and experimental lithium halides in the rocksalt crystal structure, for XC functionals with defined D3(BJ) parameters. D3(BJ) dispersion energy was included in these calculations. Values closer to zero match experiment better.

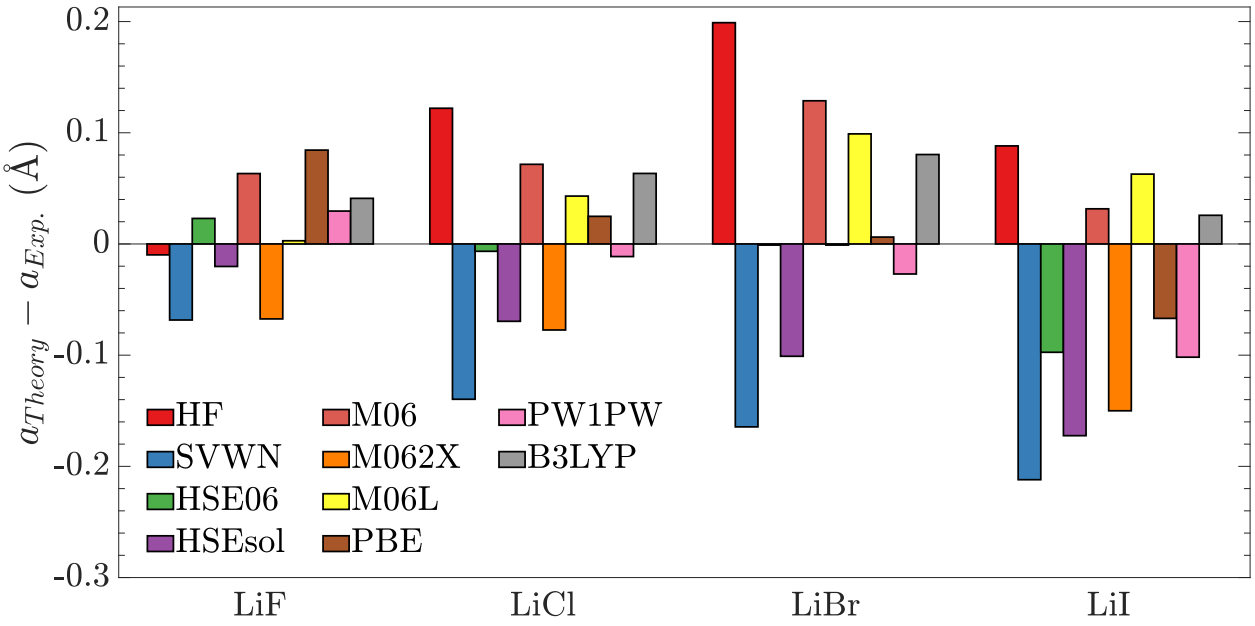

Figure 6: A comparison of the difference in lattice constant a between theoretical and experimental[63] lithium halides in the rocksalt crystal structure. D3(BJ) dispersion energy was not included in these calculations. Values closer to zero match experiment better.

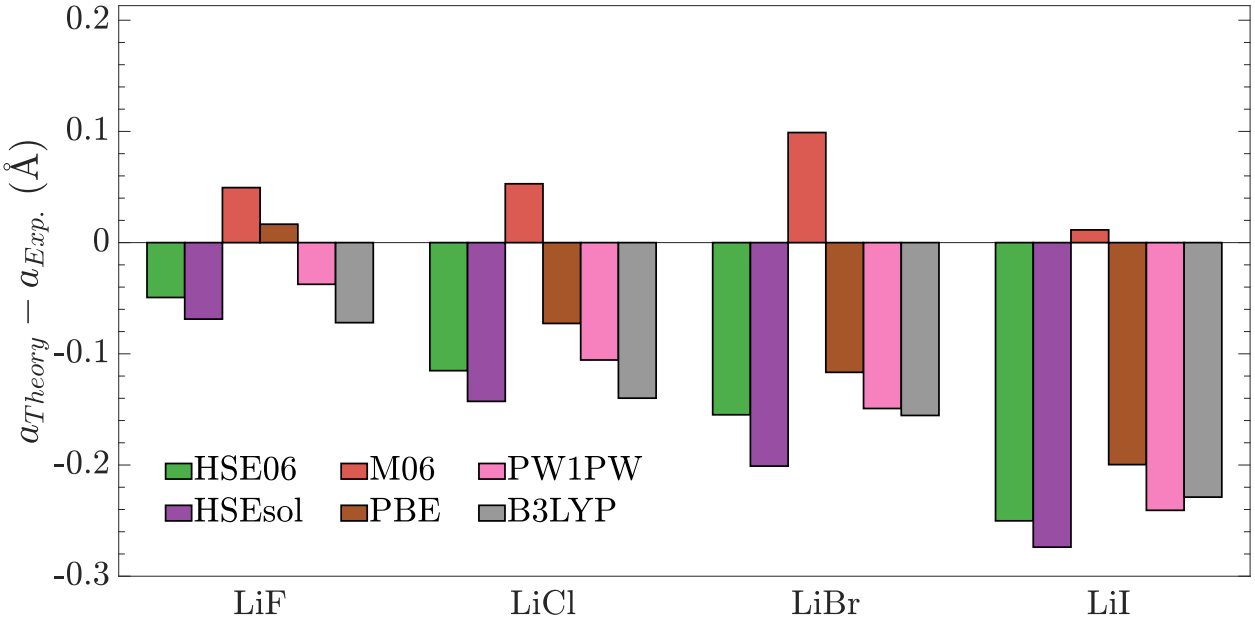

Figure 7: A comparison of the difference in lattice constant a between theoretical and experimental[63] lithium halides in the rocksalt crystal structure, for XC functionals with defined D3(BJ) parameters. D3(BJ) dispersion energy was included in these calculations. Values closer to zero match experiment better.

2.2 Empirical Energy Calculations

In order to calculate lattice energies from the TF and JC empirical models, the GROMACS (Groningen Machine for Chemical Simulations) software package version 2018[64,65] was used. GROMACS allows the calculation of single point lattice energies for any arbitrary input model and geometry. To calculate true lattice energies, GROMACS is capable of utilizing Ewald summation for ionic interactions through the particle-mesh Ewald technique.[65] The Ewald summation technique breaks down the calculation of the Coulombic energy into real-space and reciprocal-space components, which are added together to determine the total Coulombic interaction. The calculation of van der Waals (vdW) energies (e.g. the Lennard-Jones term in the JC model) is done only in direct space, with a cutoff radius sufficiently large to capture the total energy. For my lattice energy calculations, the cutoff radius was set to 2.0 nm for both the vdW interaction and for the separation between real space and reciprocal space for Ewald summation.

In order to find the optimal geometry of the TF and JC models, we calculated lattice energies of all lithium halides in the wurtzite and rocksalt crystal structures for a series of increasing lattice parameter a, with fixed fractional coordinates for the ions. Symmetry constrains the entire unit

cell for both wurtzite and rocksalt, so this was equivalent to scaling the volume of the unit cell. The lowest energy point on this potential energy curve corresponds to the equilibrium geometry of the structure. A comparison of the potential energy curves generated from this technique are compared to ab initio calculations in Fig. 8 below.

2.3 Additional Candidate Crystal Structures

In order to determine the global lowest energy crystal structure of a compound theoretically, it is necessary to explore the entire phase space of possible lattice structures. Fortunately, a fairly extensive theoretical study of the candidate structures of all alkali halides was performed by Jansen et al.[66] In light of this, I explored the possibility of a lower energy crystal structure for all lithium halides in both DFT calculations and classical ones using the TF and JC models. I tested all seven of their reported candidate structures: rocksalt, wurtzite, β-BeO, CsCl, 5-5, NiAs, and Sphalerite. The results are given below. See Ref. 66 for details of these crystal structures.

3 Results and Discussion

3.1 Comparison of Equilibrium Lattice Energies

Potential energy curves for selected ab initio and empirical calculations are shown in Fig. 8 as a function of lattice parameter a. The nonphysical dips in the DFT potential energy surfaces seen at lattice parameters far from the well minimum are due to the method by which the D3(BJ) dispersion correction is calculated. It is clear from these images that the TF model is a much better fit to ab initio data at small a (high pressures), even though it incorrectly predicts wurtzite as the lowest energy crystal structure.

In Tables 3 to 6, we report the favoured structure at the equilibrium geometry, based on the lowest lattice energy. In addition to this, the lattice energies of all lithium halides are shown for all structure types considered with the lowest lattice energy shown in bold for each calculation type. In these tables, we compare vibrationally-corrected experimental values with DFT calculations using the PBE, PW1PW, and B3LYP XC functionals (including D3(BJ) dispersion corrections), as well as classical calculations with the TF and JC models. In all cases, DFT calculations favour the

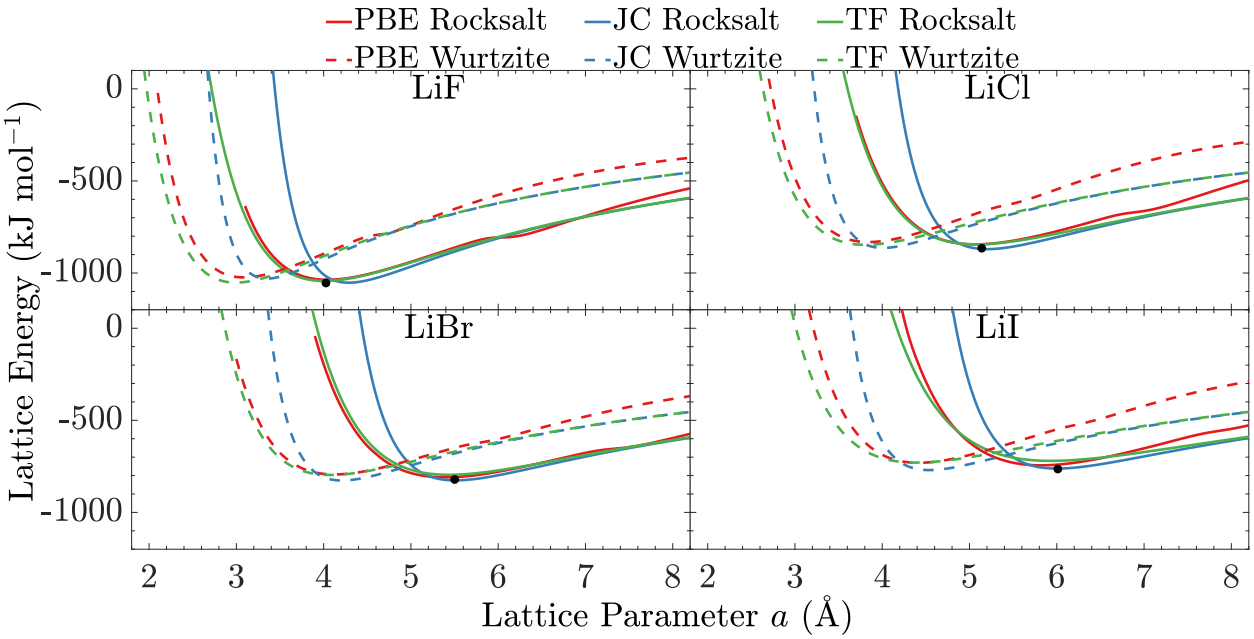

Figure 8: Comparison of rocksalt and wurtzite potential energy surfaces generated from DFT calculations (with the PBE XC functional and D3(BJ) dispersion) and JC/TF models. Corrected experimental data points[63] are included as black circles.

	Fav.	a_{Rock}	Rock.	Wurtz.	β-BeO	CsCl	5-5	NiAs	Sphal.
Exp.	Rock.	4.02620(5)	**-1054(1)**						
PBE	Rock.	4.04	**-1036.90**	-1024.37	-1021.32	-981.52	-1027.44	-1027.70	-1022.02
PW1PW	Rock.	3.99	**-1061.05**	-1046.17	-1042.99	-1003.47	-1050.28	-1051.43	-1043.95
B3LYP	Rock.	4.27	**-1075.33**	-1063.32	-1055.44	-1016.74	-1063.32	-1066.40	-1056.81
JC	Rock.	4.29	**-1052.59**	-1030.51	-1026.39	-986.38	-1041.87	-1012.94	-1028.28
TF	Wurtz.	4.01	-1043.11	**-1051.97**	-1047.51	-988.48	-1046.61	-997.53	-1049.83

Table 3: Comparison of 0 K lattice energies and rocksalt lattice parameters for the LiF salt using different theory and structure types.

experimental rocksalt structure, though other structures (e.g. NiAs structure in LiCl) are sometimes extremely close in energy. The JC and TF potentials usually predict wurtzite as the lowest energy structure, with no lower energy structures found besides rocksalt.

While performing ab initio calculations of rocksalt and wurtzite crystal structures, a subtle trend became apparent. Whenever D3(BJ) dispersion was introduced, the relative equilibrium lattice energies of all salts shifted slightly in favour of rocksalt. This initiated an idea to simply

	Fav.	a_{Rock}	Rock.	Wurtz.	β-BeO	CsCl	5-5	NiAs	Sphal.
Exp.	Rock.	5.13988(4)	**-865(2)**						
PBE	Rock.	5.07	**-844.43**	-831.97	-826.67	-791.00	-831.90	-840.53	-831.05
PW1PW	Rock.	5.03	**-856.98**	-843.53	-838.56	-801.13	-844.13	-853.26	-842.74
B3LYP	Rock.	5.03	**-866.87**	-853.33		-806.03	-851.21	-862.14	-852.47
JC	Rock.	5.20	**-870.32**	-863.58	-860.36	-792.81	-865.96	-834.62	-861.72
TF	Wurtz.	5.08	-844.73	**-846.90**	-843.22	-795.85	-843.73	-810.75	-845.13

Table 4: Comparison of 0 K lattice energies and rocksalt lattice parameters for the LiCl salt using different theory and structure types.

	Fav.	a_{Rock}	Rock.	Wurtz.	β-BeO	CsCl	5-5	NiAs	Sphal.
Exp.	Rock.	5.501(6)	**-821(2)**						
PBE	Rock.	5.38	**-810.46**	-794.35	-789.67	-757.43	-795.16	-806.96	-793.58
PW1PW	Rock.	5.35	**-823.43**	-806.07	-801.37	-767.80	-807.09	-820.12	-805.50
B3LYP	Rock.	5.35	**-829.67**	-812.85		-768.67	-811.54	-825.59	-812.37
JC	Wurtz.	5.51	-826.03	**-826.78**	-823.80	-741.36	-824.13	-790.49	-825.00
TF	Wurtz.	5.44	-795.68	**-796.72**	-793.16	-746.68	-793.70	-763.86	-795.04

Table 5: Comparison of 0 K lattice energies and rocksalt lattice parameters for the LiBr salt using different theory and structure types.

	Fav.	$a_{Rocksalt}$	Rock.	Wurtz.	β-BeO	CsCl	5-5	NiAs	Sphal.
Exp.	Rock.	6.012(7)	**-764(1)**						
PBE	Rock.	5.81	**-744.65**	-731.02	-724.64	-684.34	-728.40	-743.63	-730.58
PW1PW	Rock.	5.77	**-770.15**	-755.31	-748.32	-704.58	-752.35	-769.06	-755.02
B3LYP	Rock.	5.78	**-772.55**	-757.90		-702.49	-752.38		-757.72
JC	Wurtz.	6.00	-761.78	**-770.20**	-767.55	-674.85	-762.24	-727.50	-768.54
TF	Wurtz.	5.93	-720.06	**-729.49**	-726.76	-672.33	-722.25	-690.68	-728.00

Table 6: Comparison of 0 K lattice energies and rocksalt lattice parameters for the LiI salt using different theory and structure types.

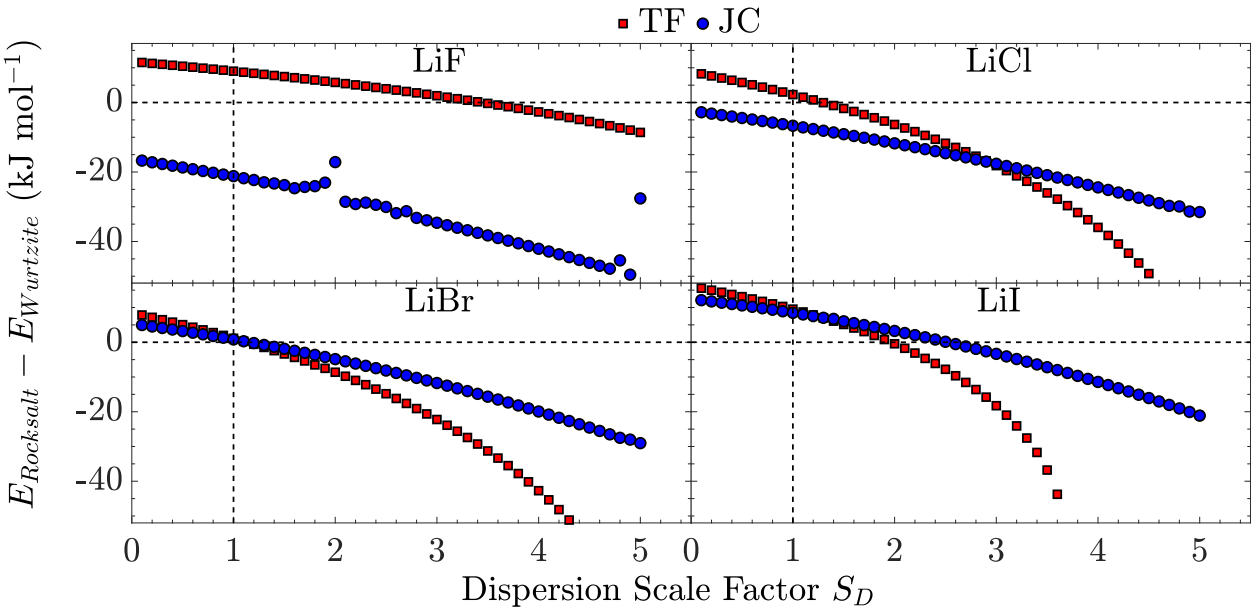

Figure 9: A plot of the difference between the equilibrium lattice energy of rocksalt and wurtzite crystal structures for both JC and TF models as a function of a simple dispersion scaling parameter.

scale the dispersion parameters of the JC and TF potentials by a factor S_D as

$$u_{ij}^{JC} = \frac{1}{4\pi\varepsilon_0}\frac{q_i q_j}{r} + 4\epsilon\left[\left(\frac{\sigma_{ij}}{r}\right)^{12} - S_D\left(\frac{\sigma_{ij}}{r}\right)^{6}\right] \tag{16}$$

$$u_{ij}^{TF} = \frac{1}{4\pi\varepsilon_0}\frac{q_i q_j}{r} + B_{ij}e^{-\alpha_{ij}r} - S_D\left(\frac{C_{ij}}{r^6} + \frac{D_{ij}}{r^8}\right). \tag{17}$$

We then recalculated the differences in lattice energy between the rocksalt and wurtzite crystal structures for various values of S_D between 0 and 5. The results of this calculation are shown in Fig. 9. An unmistakable trend is apparent, wherein increased dispersion favours the rocksalt crystal structure. This fact could be the key to explaining why so many calculations predict the wrong crystal structure in the lithium halides: the dispersion interaction is weak and difficult to capture correctly. Hence, it is often approximated poorly. Our results indicate that proper modeling of the dispersion interaction may be critical to proper structure prediction in lithium halides.

4 Ongoing and future work

After finishing our exploration of the lithium halide crystal structures through ab initio methods, the next step is to reparametrize the existing empirical models to fit the DFT data, as well as to fit experimental solubilities. If this is not possible, we will be forced to create new empirical models with different characteristics (such as non-additivity of model parameters) to match the ab initio/solubility results. Such a modification would increase the computational complexity of any MD simulations, but this may be necessary to correctly model non-classical nucleation mechanisms in lithium halides. After improving the models, the next step will be to elucidate the mechanism of lithium halide nucleation in water through MD simulation. Preliminary studies[3] have already found that strong ion hydration may impose a second free energy barrier to nucleation. The characteristics of this additional free energy barrier will be a topic of my future research.

Related to this area of research, there is a peculiar property of lithium fluoride that has been confirmed experimentally:[67] while most salts increase in solubility at higher temperature, lithium fluoride solubility in (high pressure) water decreases above 475 K. The mechanism for this phenomena is currently unknown, but is a well-suited question for me to consider.

References

[1] Karthika, S.; Radhakrishnan, T. K.; Kalaichelvi, P. A Review of Classical and Nonclassical Nucleation Theories. *Crystal Growth & Design* **2016**, *16*, 6663–6681.

[2] Lanaro, G.; Patey, G. N. Birth of NaCl Crystals: Insights from Molecular Simulations. *The Journal of Physical Chemistry B* **2016**, *120*, 9076–9087.

[3] Lanaro, G.; Patey, G. N. The influence of ion hydration on nucleation and growth of LiF crystals in aqueous solution. *The Journal of Chemical Physics* **2018**, *148*, 024507.

[4] Joung, I. S.; Cheatham, T. E. Determination of Alkali and Halide Monovalent Ion Parameters for Use in Explicitly Solvated Biomolecular Simulations. *The Journal of Physical Chemistry B* **2008**, *112*, 9020–9041.

[5] Tosi, M. P.; Fumi, F. G. Ionic sizes and born repulsive parameters in the NaCl-type alkali halides II: The generalized Huggins-Mayer form. *Journal of Physics and Chemistry of Solids* **1964**, *25*, 45–52.

[6] Berendsen, H.; Grigera, J.; Straatsma, T. The missing term in effective pair potentials. *Journal of Physical Chemistry* **1987**, *91*, 6269–6271.

[7] Slater, J. C. The Normal State of Helium. *Physical Review* **1928**, *32*, 349–360.

[8] Bach, A.; Fischer, D.; Jansen, M. Synthesis of a New Modification of Lithium Chloride Confirming Theoretical Predictions. *Zeitschrift für anorganische und allgemeine Chemie* **2009**, *635*, 2406–2409.

[9] Liebold-Ribeiro, Y.; Fischer, D.; Jansen, M. Experimental substantiation of the "energy landscape concept" for solids: synthesis of a new modification of LiBr. *Angewandte Chemie International Edition* **2008**, *47*, 4428–4431.
[10] Fischer, D.; Mueller, A.; Jansen, M. Existiert eine Wurtzit-Modifikation von Lithiumbromid?—Untersuchungen im System LiBr/LiI—. *Zeitschrift für anorganische und allgemeine Chemie* **2004**, *630*, 2697–2700.
[11] Lanaro, G.; Patey, G. N. Crystal structures of model lithium halides in bulk phase and in clusters. *Journal of Chemical Physics* **2017**, *146*.
[12] Fumi, F.; Tosi, M. Ionic sizes and born repulsive parameters in the NaCl-type alkali halides I: The Huggins-Mayer and Pauling forms. *Journal of Physics and Chemistry of Solids* **1964**, *25*, 31–43.
[13] Ladd, M.; Lee, W. The calculation of lattice energies. *Journal of Inorganic and Nuclear Chemistry* **1959**, *11*, 264–271.
[14] Rumble, J. *CRC handbook of chemistry and physics, 99th Edition*; CRC press, 2019.
[15] Huggins, M. L. Lattice Energies, Equilibrium Distances, Compressibilities and Characteristic Frequencies of Alkali Halide Crystals. *The Journal of Chemical Physics* **1937**, *5*, 143–148.
[16] Jenkins, H. D. B. Thermodynamics of the Relationship between Lattice Energy and Lattice Enthalpy. *Journal of Chemical Education* **2005**, *82*, 950.
[17] Ladd, M.; Lee, W. The calculation of lattice energies. *Journal of Inorganic and Nuclear Chemistry* **1959**, *11*, 264–271.
[18] Chase Jr, M. NIST-JANAF thermochemical tables fourth edition. *J. Phys. Chem. Ref. Data, Monograph* **1998**, *9*.
[19] Szabo, A.; Ostlund, N. S. *Modern quantum chemistry: introduction to advanced electronic structure theory*; Courier Corporation, 2012.
[20] Pascale, F.; Zicovich-Wilson, C. M.; Lopez Gejo, F.; Civalleri, B.; Orlando, R.; Dovesi, R. The calculation of the vibrational frequencies of crystalline compounds and its implementation in the CRYSTAL code. *Journal of computational chemistry* **2004**, *25*, 888–897.
[21] Zicovich-Wilson, C.; Pascale, F.; Roetti, C.; Saunders, V.; Orlando, R.; Dovesi, R. Calculation of the vibration frequencies of α-quartz: The effect of Hamiltonian and basis set. *Journal of computational chemistry* **2004**, *25*, 1873–1881.
[22] Hohenberg, P.; Kohn, W. Inhomogeneous electron gas. *Physical review* **1964**, *136*, B864.
[23] Kohn, W.; Sham, L. J. Self-consistent equations including exchange and correlation effects. *Physical review* **1965**, *140*, A1133.
[24] Dovesi, R.; Erba, A.; Orlando, R.; Zicovich-Wilson, C. M.; Civalleri, B.; Maschio, L.; Rérat, M.; Casassa, S.; Baima, J.; Salustro, S.; Kirtman, B. Quantum-mechanical condensed matter simulations with CRYSTAL. *Wiley Interdisciplinary Reviews: Computational Molecular Science* **2018**, *8*, e1360.
[25] Dovesi, R. et al. CRYSTAL17 User's Manual. *University of Torino* **2017**,
[26] Peintinger, M. F.; Oliveira, D. V.; Bredow, T. Consistent Gaussian basis sets of triple-zeta valence with polarization quality for solid-state calculations. *Journal of Computational Chemistry* **2013**, *34*, 451–459.
[27] Tosoni, S.; Tuma, C.; Sauer, J.; Civalleri, B.; Ugliengo, P. A comparison between plane wave and Gaussian-type orbital basis sets for hydrogen bonded systems: Formic acid as a test case. *The Journal of chemical physics* **2007**, *127*, 154102.
[28] Laun, J.; Vilela Oliveira, D.; Bredow, T. Consistent gaussian basis sets of double- and triple-zeta valence with polarization quality of the fifth period for solid-state calculations. *Journal of Computational Chemistry* **2018**, *39*, 1285–1290.
[29] Bredow, T.; Gerson, A. R. Effect of exchange and correlation on bulk properties of MgO, NiO,

and CoO. *Phys. Rev. B* **2000**, *61*, 5194–5201.
[30] Rappoport, D.; Furche, F. Property-optimized Gaussian basis sets for molecular response calculations. *The Journal of Chemical Physics* **2010**, *133*, 134105.
[31] Ojamäe, L.; Hermansson, K.; Pisani, C.; Causà, M.; Roetti, C. Structural, vibrational and electronic properties of a crystalline hydrate from ab initio periodic Hartree–Fock calculations. *Acta Crystallographica Section B: Structural Science* **1994**, *50*, 268–279.
[32] Nada, R.; Catlow, C.; Pisani, C.; Orlando, R. An ab-initio Hartree-Fock perturbed-cluster study of neutral defects in LiF. *Modelling and Simulation in Materials Science and Engineering* **1993**, *1*, 165.
[33] Apra, E.; Causa, M.; Prencipe, M.; Dovesi, R.; Saunders, V. On the structural properties of NaCl: an ab initio study of the B1-B2 phase transition. *Journal of Physics: Condensed Matter* **1993**, *5*, 2969.
[34] Doll, K.; Stoll, H. Ground-state properties of heavy alkali halides. *Physical Review B* **1998**, *57*, 4327.
[35] Hehre, W.; Lathan, W.; Ditchfield, R.; Newton, M. Program No. 236, Quantum Chemistry Program Exchange, Indiana University, Bloomington, Indiana;(b) WJ Hehre, RF Stewart, and JA Pople. *J. Chem. Phys* **1969**, *2*, 2657.
[36] Hehre, W. R. Ditchfield, RF Stewart, and JA Pople. *J. Chem. Phys* **1970**, *52*, 2769.
[37] Pietro, W. J.; Levi, B. A.; Hehre, W. J.; Stewart, R. F. Molecular orbital theory of the properties of inorganic and organometallic compounds. 1. STO-NG basis sets for third-row main-group elements. *Inorganic Chemistry* **1980**, *19*, 2225–2229.
[38] Pietro, W. J.; Blurock, E. S.; Hout Jr, R. F.; Hehre, W. J.; DeFrees, D. J.; Stewart, R. F. Molecular orbital theory of the properties of inorganic and organometallic compounds. 2. STO-NG basis sets for fourth-row main-group elements. *Inorganic Chemistry* **1981**, *20*, 3650–3654.
[39] Perdew, J. P.; Burke, K.; Ernzerhof, M. Generalized Gradient Approximation Made Simple. *Phys. Rev. Lett.* **1996**, *77*, 3865–3868.
[40] Mardirossian, N.; Head-Gordon, M. Thirty years of density functional theory in computational chemistry: an overview and extensive assessment of 200 density functionals. *Molecular Physics* **2017**, *115*, 2315–2372.
[41] Grimme, S.; Antony, J.; Ehrlich, S.; Krieg, H. A consistent and accurate ab initio parametrization of density functional dispersion correction (DFT-D) for the 94 elements H-Pu. *The Journal of Chemical Physics* **2010**, *132*, 154104.
[42] Grimme, S.; Hansen, A.; Brandenburg, J. G.; Bannwarth, C. Dispersion-corrected mean-field electronic structure methods. *Chemical reviews* **2016**, *116*, 5105–5154.
[43] Becke, A. D.; Johnson, E. R. A unified density-functional treatment of dynamical, nondynamical, and dispersion correlations. *The Journal of Chemical Physics* **2007**, *127*, 124108.
[44] Grimme, S.; Ehrlich, S.; Goerigk, L. Effect of the damping function in dispersion corrected density functional theory. *Journal of Computational Chemistry* **2011**, *32*, 1456–1465.
[45] Dirac, P. A. M. Note on Exchange Phenomena in the Thomas Atom. *Mathematical Proceedings of the Cambridge Philosophical Society* **1930**, *26*, 376–385.
[46] Vosko, S. H.; Wilk, L.; Nusair, M. Accurate spin-dependent electron liquid correlation energies for local spin density calculations: a critical analysis. *Canadian Journal of Physics* **1980**, *58*, 1200–1211.
[47] Zhao, Y.; Truhlar, D. G. A new local density functional for main-group thermochemistry, transition metal bonding, thermochemical kinetics, and noncovalent interactions. *The Journal of Chemical Physics* **2006**, *125*, 194101.
[48] Zhao, Y.; Truhlar, D. G. The M06 suite of density functionals for main group thermochemistry, thermochemical kinetics, noncovalent interactions, excited states, and transition elements:

two new functionals and systematic testing of four M06-class functionals and 12 other functionals. *Theoretical Chemistry Accounts* **2008**, *120*, 215–241.
[49] Becke, A. D. Density-functional thermochemistry. III. The role of exact exchange. *The Journal of Chemical Physics* **1993**, *98*, 5648–5652.
[50] Becke, A. D. Density-functional exchange-energy approximation with correct asymptotic behavior. *Physical review A* **1988**, *38*, 3098.
[51] Lee, C.; Yang, W.; Parr, R. G. Development of the Colle-Salvetti correlation-energy formula into a functional of the electron density. *Physical review B* **1988**, *37*, 785.
[52] Krukau, A. V.; Vydrov, O. A.; Izmaylov, A. F.; Scuseria, G. E. Influence of the exchange screening parameter on the performance of screened hybrid functionals. *The Journal of chemical physics* **2006**, *125*, 224106.
[53] Schimka, L.; Harl, J.; Kresse, G. Improved hybrid functional for solids: The HSEsol functional. *The Journal of Chemical Physics* **2011**, *134*, 024116.
[54] Ernzerhof, M.; Perdew, J. P.; Burke, K. Coupling-constant dependence of atomization energies. *International Journal of Quantum Chemistry* **1997**, *64*, 285–295.
[55] He, L.; Liu, F.; Hautier, G.; Oliveira, M. J.; Marques, M. A.; Vila, F. D.; Rehr, J.; Rignanese, G.-M.; Zhou, A. Accuracy of generalized gradient approximation functionals for density-functional perturbation theory calculations. *Physical Review B* **2014**, *89*, 064305.
[56] Perdew, J. P.; Ruzsinszky, A.; Csonka, G. I.; Vydrov, O. A.; Scuseria, G. E.; Constantin, L. A.; Zhou, X.; Burke, K. Restoring the density-gradient expansion for exchange in solids and surfaces. *Physical review letters* **2008**, *100*, 136406.
[57] Perdew, J. P.; Wang, Y. Pair-distribution function and its coupling-constant average for the spin-polarized electron gas. *Physical Review B* **1992**, *46*, 12947.
[58] Monkhorst, H. J.; Pack, J. D. Special points for Brillouin-zone integrations. *Physical review B* **1976**, *13*, 5188.
[59] Mayer, I. Towards a "chemical" hamiltonian. *International Journal of Quantum Chemistry* **1983**, *23*, 341–363.
[60] Boys, S. F.; Bernardi, F. d. The calculation of small molecular interactions by the differences of separate total energies. Some procedures with reduced errors. *Molecular Physics* **1970**, *19*, 553–566.
[61] Kruse, H.; Grimme, S. A geometrical correction for the inter-and intra-molecular basis set superposition error in Hartree-Fock and density functional theory calculations for large systems. *The Journal of chemical physics* **2012**, *136*, 04B613.
[62] Burns, L. A.; Mayagoitia, Á. V.; Sumpter, B. G.; Sherrill, C. D. Density-functional approaches to noncovalent interactions: a comparison of dispersion corrections (DFT-D), exchange-hole dipole moment (XDM) theory, and specialized functionals. *The Journal of chemical physics* **2011**, *134*, 084107.
[63] Sirdeshmukh, D. B.; Sirdeshmukh, L.; Subhadra, K. *Alkali Halides: A Handbook of physical properties*; Springer Science & Business Media, 2013; Vol. 49.
[64] Abraham, M. J.; Murtola, T.; Schulz, R.; Páll, S.; Smith, J. C.; Hess, B.; Lindahl, E. GROMACS: High performance molecular simulations through multi-level parallelism from laptops to supercomputers. *SoftwareX* **2015**, *1*, 19–25.
[65] Lindahl, E.; Hess, B.; Abraham, M.; van der Spoel, D.; the GROMACS development team, GROMACS Reference Manual Version 2018. www.gromacs.org, 2018.
[66] Čančarević, Ž. P.; Schoen, J. C.; Jansen, M. Stability of alkali metal halide polymorphs as a function of pressure. *Chemistry–An Asian Journal* **2008**, *3*, 561–572.
[67] Booth, H. S.; Bidwell, R. M. Solubilities of Salts in Water at High Temperatures. *J. Am. Chem. Soc.* **1950**, *72*, 2567.